



Title	Selective oxidation of n-butane over nanosized crystallites of (VO) <sub>2</sub> P <sub>2</sub> O <sub>7</sub> synthesized by an exfoliation-reduction process of VOPO <sub>4</sub> ·2H <sub>2</sub> O in a mixture of 2-butanol and ethanol
Author(s)	Imai, Hiroyuki; Kamiya, Yuichi; Okuhara, Toshio
Citation	Journal of Catalysis, 251(1), 195-203 <a href="https://doi.org/10.1016/j.jcat.2007.06.026">https://doi.org/10.1016/j.jcat.2007.06.026</a>
Issue Date	2007-10-01
Doc URL	<a href="http://hdl.handle.net/2115/30184">http://hdl.handle.net/2115/30184</a>
Type	article (author version)
File Information	JOC251-1.pdf



[Instructions for use](#)

Revised manuscript (JCAT07-377)

**Selective oxidation of *n*-butane over nano-sized crystallites of  $(VO)_2P_2O_7$   
synthesized by an exfoliation-reduction process of  $VOPO_4 \cdot 2H_2O$   
in a mixture of 2-butanol and ethanol**

Hiroyuki Imai, Yuichi Kamiya\*, Toshio Okuhara\*

*Research Faculty of Environmental Earth Science, Hokkaido University,*

*Sapporo 060-0810, Japan*

\*Corresponding authors

Y. Kamiya

Tel/Fax: +81-11-706-4513

E-mail: kamiya@ees.hokudai.ac.jp

T. Okuhara

Tel/Fax: +81-11-706-4513

E-mail: oku@ees.hokudai.ac.jp

## Abstract

Intercalation, exfoliation, and reduction of  $\text{VOPO}_4 \cdot 2\text{H}_2\text{O}$  were conducted in 2-butanol alone and in a mixed alcohol solvent (2-butanol and ethanol). While both processes produced crystallites of pure  $\text{VOHPO}_4 \cdot 0.5\text{H}_2\text{O}$ , much smaller and thinner crystallites (av.  $340 \text{ nm} \times 35 \text{ nm}$ ) were formed in the mixed alcohol compared with 2-butanol alone (av.  $950 \text{ nm} \times 200 \text{ nm}$ ). The small, thin crystallites of precursor  $\text{VOHPO}_4 \cdot 0.5\text{H}_2\text{O}$  could be transformed into sharply angular nano-sized crystallites (60 nm in length and 31 nm in thickness) of highly crystalline  $(\text{VO})_2\text{P}_2\text{O}_7$ , without mesopores. When used as a catalyst, this compound exhibited higher activity and selectivity to maleic anhydride (75% at 80% conversion) for selective oxidation of *n*-butane than that derived from the precursor prepared in 2-butanol alone. The high activity of the nano-sized crystallites of  $(\text{VO})_2\text{P}_2\text{O}_7$  is attributed to their large surface area ( $40 \text{ m}^2 \text{ g}^{-1}$ ), which is due to their smaller dimensions, and their high selectivity may be attributed to the lack of mesopores as well as their highly crystalline state.

*Keywords: n-butane oxidation;  $(\text{VO})_2\text{P}_2\text{O}_7$ ; nano-crystallites; exfoliation; morphology*

## 1. Introduction

Although the selective oxidation of *n*-butane to maleic anhydride (MA) has been commercialized using vanadyl pyrophosphate  $(VO)_2P_2O_7$  as a catalyst [1-3], low selectivity toward MA remains a serious problem. Therefore, it is keenly desirable to develop new and functional forms of  $(VO)_2P_2O_7$  which can offer an improvement to this oxidation process.

Previous studies have demonstrated that selectivity in this reaction is sensitive to the chemical and physical properties of  $(VO)_2P_2O_7$  crystallites, including microstructure, defect sites, composition, oxidation state, and the presence of  $VOPO_4$  phases [4-6]. Among these factors, the microstructure (shape and dimension) of the  $(VO)_2P_2O_7$  crystallites is considered to have a critical effect on selectivity in *n*-butane oxidation [4]. Thus, control of the shape and dimension of  $(VO)_2P_2O_7$  crystallites should result in an improvement in catalytic performance.

The  $(VO)_2P_2O_7$  catalyst is normally synthesized from the precursor  $VOHPO_4 \cdot 0.5H_2O$  [1,2,7,8]. Various preparation methods for this precursor have been investigated, and these are generally categorized into three types: preparation in aqueous solution [9], preparation in an organic solvent [10], and preparation by direct reduction of layered  $VOPO_4 \cdot 2H_2O$  with alcohol [11].  $(VO)_2P_2O_7$  prepared by the organic solvent method is known to be a highly active and selective catalyst [1,2]. In fact, commercial  $(VO)_2P_2O_7$  catalysts are prepared by this method, although the catalytic performance, especially in terms of selectivity to MA, is still

unsatisfactory.

$\text{VOPO}_4 \cdot 2\text{H}_2\text{O}$ , which is a starting material for the direct reduction method, possesses a layered structure with a high capability for intercalation of various molecules [12]. We previously succeeded in carrying out exfoliation of  $\text{VOPO}_4 \cdot 2\text{H}_2\text{O}$  in various alcohols [13], and demonstrated that subsequent reduction of the exfoliated  $\text{VOPO}_4$  sheets with alcohol produced  $\text{VOHPO}_4 \cdot 0.5\text{H}_2\text{O}$ . In particular, as we described in a preliminary report [14],  $(\text{VO})_2\text{P}_2\text{O}_7$  catalyst derived from  $\text{VOHPO}_4 \cdot 0.5\text{H}_2\text{O}$  which had been prepared by exfoliation-reduction of  $\text{VOPO}_4 \cdot 2\text{H}_2\text{O}$  in a mixed alcohol solvent (2-butanol and ethanol) was found to be superior, in terms of activity and selectivity, to the catalyst derived from  $\text{VOHPO}_4 \cdot 0.5\text{H}_2\text{O}$  prepared in 2-butanol alone and by the direct-reduction method for *n*-butane oxidation [15].

In the present study, we investigated the influence of ethanol on the microstructure of the precursor  $\text{VOHPO}_4 \cdot 0.5\text{H}_2\text{O}$  prepared by the exfoliation-reduction of  $\text{VOPO}_4 \cdot 2\text{H}_2\text{O}$  in a mixture of 2-butanol and ethanol. The precursors were prepared systematically in solvents containing varying amounts of ethanol, and were characterized by means of X-ray diffraction, IR spectroscopy, X-ray photoelectron spectroscopy,  $\text{N}_2$  adsorption-desorption isotherms, scanning electron microscopy, and redox titration. Furthermore, the catalytic performance of the resulting compounds is discussed with reference to their microstructures.

## 2. Experimental

### 2.1. Materials

#### 2.1.1. $\text{VOPO}_4 \cdot 2\text{H}_2\text{O}$

$\text{VOPO}_4 \cdot 2\text{H}_2\text{O}$  was prepared according to the method described in the literature [16]. A mixture of  $\text{V}_2\text{O}_5$  (24 g, Wako Pure Chem. Ind., Ltd.), aqueous 85%  $\text{H}_3\text{PO}_4$  (223 g, Wako Pure Chem. Ind., Ltd.) and  $\text{H}_2\text{O}$  ( $577 \text{ cm}^3$ ) was refluxed for 16 h. The resulting precipitate was separated by filtration, washed with acetone, and dried under ambient atmosphere. The resulting yellow solid was identified as  $\text{VOPO}_4 \cdot 2\text{H}_2\text{O}$  by XRD and IR spectroscopy [16].

#### 2.1.2. $\text{VOHPO}_4 \cdot 0.5\text{H}_2\text{O}$

The precursor  $\text{VOHPO}_4 \cdot 0.5\text{H}_2\text{O}$  was prepared by exfoliation-reduction of  $\text{VOPO}_4 \cdot 2\text{H}_2\text{O}$  in a mixture of 2-butanol and ethanol, with different products obtained depending on the amount of ethanol added. Details of the exfoliation-reduction process were reported previously [13]. A mixture of  $\text{VOPO}_4 \cdot 2\text{H}_2\text{O}$  (2.0 g) and 2-butanol ( $50 \text{ cm}^3$ , Wako Pure Chem. Ind., Ltd.) was heated stepwise to 303, 323, 343, and 363 K and maintained for 1 h at each temperature with stirring to form a homogeneous solution containing exfoliated  $\text{VOPO}_4$  sheets as the product of intercalation followed by exfoliation [13]. After the exfoliation process, to the resulting homogeneous 2-butanol solution at room temperature, ethanol ( $7 \sim 50 \text{ cm}^3$ , Wako Pure Chem.

Ind., Ltd.) was added, and this solution was refluxed for 20 h (reduction) to form a light-blue precipitate. The precipitate was separated by centrifugation, washed with acetone, and dried at room temperature overnight to obtain the precursor  $\text{VOHPO}_4 \cdot 0.5\text{H}_2\text{O}$ . Henceforth the precursors are denoted as EP- $x$ , in which  $x$  represents the additional amount ( $\text{cm}^3$ ) of ethanol added to the 2-butanol solution. The precursor EP-0 was also prepared by exfoliation-reduction in 2-butanol alone.

## 2.2 Characterization

The powder XRD patterns of the solid samples were measured on an XRD diffractometer (Miniflex, Rigaku) with  $\text{CuK}\alpha$  radiation. IR spectra of solid samples were measured as KBr disks using a FT-IR-230 (JASCO). The adsorption-desorption isotherms of nitrogen were measured at 77 K using an automatic adsorption apparatus (BELSORP 28SA, BEL Japan Inc.) after the precursors and catalysts were evacuated at 423 and 523 K, respectively. Specific surface area and mesopore size distributions were calculated by the BET and DH method, respectively.

Scanning electron microscope (SEM) images were obtained using a FE-SEM S-4800 (Hitachi). The average oxidation number of V in the sample bulk was determined by a redox-titration method with  $\text{KMnO}_4$  [17]. X-ray photoelectron spectra (XPS) were obtained

using a Shimadzu XPS-7000 with  $MgK_{\alpha}$  radiation. The P/V atomic ratio of the surface was estimated using the method reported in ref. [18]. Elemental analysis of the compound was performed by Mikroanalytisches Labor Pascher (Germany) for V, P, C, and H. The content of oxygen in the sample was calculated by subtracting the sum of weights of V, P, C, and H.

### 2.3. Catalytic oxidation of *n*-butane

Selective oxidation of *n*-butane was carried out at 703 K in a flow reactor (Pyrex tube, 10 mm inner diameter) under atmospheric pressure. The catalyst precursor (185 mg) was placed in the reactor, and then the reactant gas, consisting of *n*-butane (1.5 vol%), O<sub>2</sub> (17 vol%) and He (balance) was fed at a rate of 10 cm<sup>3</sup> min<sup>-1</sup>. The temperature was raised to 703 K at a rate of 5 K min<sup>-1</sup>, and when this temperature was reached, the gas from the reactor outlet was analyzed using on-line gas chromatography. An FID-GC (Shimadzu GC8A) with a Porapak QS column (1 m) was used for analysis of *n*-butane and MA. A high-speed GC (Agilent 3000A) with Porapak Q and molecular sieve 5A columns was used for analysis of CO, CO<sub>2</sub> and O<sub>2</sub> in the gas phase.

Since conversion and selectivity in the reaction changed gradually over time, the  $W/F$  dependence ( $W$  is weight of the catalyst, and  $F$  the total flow rate) was measured by changing the total flow rate after stationary conversion and selectivity were reached; this occurred after

the reaction had proceeded for at least 150 h. In this study, samples showing stationary conversion and selectivity are considered as catalysts. The catalyst derived from EP-*x* is denoted EC-*x*.

### 3. Results

#### 3.1. Microstructures of precursors and catalysts

The XRD patterns of the precursors are shown in Fig. 1. All of the precursors except for EP-50 exhibited patterns attributed to the  $\text{VOHPO}_4 \cdot 0.5\text{H}_2\text{O}$  phase, but the relative intensities and line widths of the diffraction lines were different, varying with the amount of ethanol added. The intensity of the (001) line decreased as the amount of ethanol increased, while changes in the intensity and line width of the (220) line were small. EP-15 and EP-36 showed broad, weak (001) lines (Figs. 1c and d). EP-50 gave a diffraction line at  $11.36^\circ$  of  $2\theta$  (0.78 nm) and a weak line at  $15.22^\circ$  (0.58 nm), which were assignable to the (002) and (003) reflections of the lamellar phase, respectively (Fig. 1e). Elemental analysis of EP-50 showed that the carbon content was 10.5 wt% for EP-50, ethanol contained in the interlayer space of the lamellar phase.

Figure 2 shows the IR spectra of the precursors. All spectra, except for that of EP-50, were consistent with that reported previously for  $\text{VOHPO}_4 \cdot 0.5\text{H}_2\text{O}$  [10]:  $1199$ ,  $1104$ , and  $1052$   $\text{cm}^{-1}$  [ $\nu(\text{PO}_3)$ ],  $1132$   $\text{cm}^{-1}$  [ $\delta(\text{P-OH})$ ],  $977$   $\text{cm}^{-1}$  [ $\nu(\text{V=O})$ ],  $931$   $\text{cm}^{-1}$  [ $\nu(\text{P-OH})$ ],  $799$   $\text{cm}^{-1}$

[ $\nu(\text{V-O}=\text{V})$ ], and  $743\text{ cm}^{-1}$  [ $\nu(\text{P-O-P})$ ]. All of the IR spectra were very similar to each other and these precursors were highly crystalline. EP-50 showed broad bands in this region (Fig. 2e).

SEM images of the precursors and the starting material  $\text{VOPO}_4 \cdot 2\text{H}_2\text{O}$  are shown in Fig. 3. This figure also shows the size distributions of the crystallites estimated from the SEM images; about 500 crystallites were randomized on the SEM images and the lengths of each crystallite were measured. As described previously [15,16],  $\text{VOPO}_4 \cdot 2\text{H}_2\text{O}$  consisted of square platelet particles with length of about  $20\ \mu\text{m}$  (Fig. 3f). However, the shapes and lengths of the catalyst precursors were significantly different from those of the starting  $\text{VOPO}_4 \cdot 2\text{H}_2\text{O}$ , and varied depending on the amount of ethanol added. The lengths of the crystallites of EP-0 were widely distributed in the range  $0.2 - 2.8\ \mu\text{m}$ , with an average length of  $0.95\ \mu\text{m}$  (Fig. 3a); however, for the precursors formed in a 2-butanol/ethanol mixture, much smaller and more uniformly sized crystallites were observed. In particular, EP-36 had the smallest nano-sized crystallites, with an average length of  $0.34\ \mu\text{m}$  and thickness of  $35\ \text{nm}$  (Table 1).

Table 1 summarizes the surface area, average length and thickness of the crystallites, oxidation number of V in the bulk, and P/V atomic ratio of the surface for all of the precursors. The thicknesses were estimated using Eq. (1):

$$\frac{2}{t} + \frac{4}{L} = S\rho \quad (1)$$

Here,  $t$  (m) is the thickness of the crystallite,  $L$  (m) the length of the crystallite,  $S$  ( $\text{m}^2 \text{g}^{-1}$ ) the surface area, and  $\rho$  the density ( $2.822 \times 10^6 \text{ g m}^{-3}$ ) of  $\text{VOHPO}_4 \cdot 0.5\text{H}_2\text{O}$  and it was assumed that the crystallite was a rectangular solid, in which the size and thickness were  $L$  and  $t$ , respectively. The surface area monotonically increased with the amount of ethanol added up to  $36 \text{ cm}^3$  (EP-36). The thickness of the precursors followed the order  $\text{EP-0} > \text{EP-7} > \text{EP-15} > \text{EP-36}$ ; EP-36 was about six times thinner than EP-0. The oxidation number of V was about 4.0 regardless of the amount of ethanol added. The surface P/V ratios of the precursors  $\text{VOHPO}_4 \cdot 0.5\text{H}_2\text{O}$  were close to 1.0.

Figure 4 shows the XRD patterns of the catalysts after 150 h of reaction. All the catalysts except for EC-50 showed the patterns of the  $(\text{VO})_2\text{P}_2\text{O}_7$  phase [19], but the relative intensity and broadness varied depending on the amount of ethanol added. EC-50 exhibited no diffraction lines, being amorphous. The P/V ratio in the bulk and average oxidation number of V for EC-50 were near unity and 4.6, respectively. The IR spectra of the catalysts are shown in Fig. 5. The spectra of all catalysts except for EC-50 were basically consistent with the spectrum of  $(\text{VO})_2\text{P}_2\text{O}_7$  [10], which was in agreement with the results obtained by XRD.

Figure 6 shows SEM images and size distributions of the catalyst particles. The apparent shapes and sizes of the crystallites of EC-0 were similar to those of the corresponding precursor EP-0 (Fig. 3a), and there was a wide size distribution (20 nm to 2000 nm). In

contrast, the catalysts derived from precursors prepared in a 2-butanol/ethanol mixture showed quite different crystallite shapes and sizes compared to the corresponding precursors; these catalysts consisted of bare, angular nano-sized crystallites with a narrow size distribution. The size of the crystallites decreased as the amount of ethanol increased. EC-36 had the smallest particle size (av. 60 nm), which was one tenth of that of EC-0. It is important to note that EC-36 is composed of only small particles.

Table 2 summarizes the surface area, length and thickness of the particles, oxidation number of V in the bulk catalyst, and surface P/V atomic ratio of the catalysts, as well as their selectivity and activity for *n*-butane oxidation; catalytic data were collected after the stationary state was reached at 703 K. The thicknesses were estimated from the surface areas and lengths of the catalyst particles [Eq. (1)] based on the density of  $(VO)_2P_2O_7$  ( $3.342 \text{ g cm}^{-3}$ ). The surface areas of the catalysts were much larger than those of the corresponding precursors, while the lengths and thicknesses of the catalyst particles were much smaller. The trends in surface area, length, and thickness in the catalysts were similar to those of the precursors. The oxidation numbers of V in the catalyst bulk were close to 4 for all catalysts except EC-50, which is consistent with the results obtained using XRD, while that of EC-50 was much larger. The surface P/V ratios slightly exceeded unity, but those of EC-0, EC-7, EC-15, and EC-36 were nearly the same (1.20 - 1.32).

Figure 7 shows the mesopore size distributions of the catalysts, estimated based on N<sub>2</sub> desorption isotherms at 77 K. A sharp peak around 4 nm was observed for EC-0. Since crystallites of (VO)<sub>2</sub>P<sub>2</sub>O<sub>7</sub> are non-porous, these mesopores may be attributed to the voids between the crystallites. In contrast, it was noted that no mesopores were observed for the catalysts derived from precursors prepared in the 2-butanol/ethanol mixture.

### 3.2. Selective oxidation of *n*-butane

Figure 8 shows the *W/F* dependence of conversion for *n*-butane oxidation at 703 K. The catalytic activities were estimated from the initial slopes of the curves. The activities of the catalysts derived from the precursors prepared in the 2-butanol/ethanol mixture (EC-7, EC-15, and EC-36) were higher than that of EC-0, while the activity per unit surface area was similar for all catalysts, as shown in Table 2. EC-50 showed very low activity and selectivity to MA (Table 2).

Figure 9 shows selectivity to MA (based on *n*-butane) plotted against the conversion of *n*-butane. It should be emphasized that selectivity to MA increased with the amount of ethanol added. The selectivity to MA of EC-36 reached about 78% at low conversions, and remained at 75% even at 80% conversion.

## 4. Discussion

### 4.1. Influence of addition of ethanol on microstructure of precursors

We previously succeeded in carrying out exfoliation of  $\text{VOPO}_4 \cdot 2\text{H}_2\text{O}$  in 2-butanol. The subsequent reduction of the exfoliated  $\text{VOPO}_4$  sheets with 2-butanol provided thinner and smaller-sized crystallites of  $\text{VOHPO}_4 \cdot 0.5\text{H}_2\text{O}$  (EP-0,  $950 \text{ nm} \times 200 \text{ nm}$ ) compared to the precursor formed by direct reduction of  $\text{VOPO}_4 \cdot 2\text{H}_2\text{O}$  with 2-butanol ( $5000 \text{ nm} \times 250 \text{ nm}$ ) [15]. In the present study, we found that the addition of ethanol to the 2-butanol solution containing the exfoliated  $\text{VOPO}_4$  sheets resulted in a further reduction in the thickness and length of the  $\text{VOHPO}_4 \cdot 0.5\text{H}_2\text{O}$  crystallites (Table 1), and a narrower size distribution (Fig. 3). In particular, EP-36 was found to be composed of nano-sized thin crystallites with a length of 340 nm and a thickness of 35 nm. These microcrystallites possessed a relatively high surface area; the surface area of EP-36 ( $24 \text{ m}^2 \text{ g}^{-1}$ ) was about five times larger than that of EP-0 ( $5 \text{ m}^2 \text{ g}^{-1}$ ). However, as shown in Fig. 1 and Table 1, the addition of ethanol had no effect on the bulk structure of the precursors (crystalline phase, crystallinity, and oxidation number of V in the bulk crystal), although addition of an excess amount of ethanol resulted in the formation of a lamellar phase (EP-50). Ultimately, it was found that ethanol affects only the morphology (size and dimension) of the crystallites, and not the crystalline structure.

The oxidation number of V in the exfoliated  $\text{VOPO}_4$  sheets was close to 5.0 [13] while

that of the  $\text{VOHPO}_4 \cdot 0.5\text{H}_2\text{O}$  material was about 4.0 (Table 1). Based on this, it was concluded that the exfoliated  $\text{VOPO}_4$  sheets were reduced, and their reduced forms (“exfoliated V-P-O sheets”) were stacked to form  $\text{VOHPO}_4 \cdot 0.5\text{H}_2\text{O}$  during the exfoliation-reduction process. In a separate experiment, the supernatant solution was evaporated to give a yellow solid just after the appearance of the precursor crystallites in the solution (5 h after the beginning of reflux), and this solid was subjected to elemental analysis. The result showed that composition of the yellow solid was 24.5, 14.8, 57.6, 2.5, and 0.56wt% for V, P, O, H, and C, respectively, which basically consistent with the composition of  $\text{VOPO}_4 \cdot 2\text{H}_2\text{O}$  (25.8, 15.7, 56.6, and 2.0 for V, P, O and H, respectively). This suggests that ethanol and its derivatives, such as esters, were not bonded to the exfoliated V-P-O sheets in the solution during the exfoliation-reduction process. Our previous report demonstrated that  $\text{VOPO}_4 \cdot 2\text{H}_2\text{O}$  did not undergo exfoliation in ethanol alone, instead forming an intercalation compound of  $\text{VOPO}_4 \cdot 2\text{H}_2\text{O}$  with ethanol. In addition, we confirmed that  $\text{VOPO}_4 \cdot 2\text{H}_2\text{O}$  was not reduced with ethanol by the direct reduction method. From these findings, it is reasonable to conclude that ethanol merely inhibits stacking of the exfoliated V-P-O sheets.

The exfoliated V-P-O sheets are solvated by both alcohols (2-butanol and ethanol) in the alcohol solution. Since molecular size of ethanol is smaller than that of 2-butanol, large amounts of alcohol molecules solvate the exfoliated V-P-O sheets when ethanol is present in the

2-butanol solution. This inhibits stacking of the exfoliated V-P-O sheets, resulting in the formation of thinner  $\text{VOHPO}_4 \cdot 0.5\text{H}_2\text{O}$  crystallites. As Fig. 3 shows, the fringes of the precursor crystallites prepared in the mixed alcohol (EP-7, EP-15, and EP-36) were unclear and jagged, while EC-0 was composed of hexagonal sharply-defined crystallites, which suggests that the crystal growth of  $\text{VOHPO}_4 \cdot 0.5\text{H}_2\text{O}$  toward the lateral direction did not progress sufficiently in the mixed alcohol. Therefore, solvation of the exfoliated V-P-O sheets by ethanol also inhibited the connection of the exfoliated V-P-O sheets, resulting in the formation of much smaller  $\text{VOHPO}_4 \cdot 0.5\text{H}_2\text{O}$  crystallites.

#### *4.2. Microstructures of catalysts derived from precursors with different crystallite sizes*

The transformation from  $\text{VOHPO}_4 \cdot 0.5\text{H}_2\text{O}$  to  $(\text{VO})_2\text{P}_2\text{O}_7$  proceeds via a complex process involving dehydration, oxidation, and reduction. Kiely et al. revealed that topotactic dehydration to  $(\text{VO})_2\text{P}_2\text{O}_7$  occurs preferentially at the periphery of the  $\text{VOHPO}_4 \cdot 0.5\text{H}_2\text{O}$  crystallites, whereas in the interior of the crystallites,  $\text{VOHPO}_4 \cdot 0.5\text{H}_2\text{O}$  was initially oxidized to  $\delta\text{-VOPO}_4$  and then reduced to  $(\text{VO})_2\text{P}_2\text{O}_7$ , with the size and shape of the precursor being retained during the transformation [20]. We also demonstrated that the crystallite size of the precursor  $\text{VOHPO}_4 \cdot 0.5\text{H}_2\text{O}$  has a significant effect on the crystallite phases and microstructure of the catalyst formed [21]; moderately sized crystallites of  $\text{VOHPO}_4 \cdot 0.5\text{H}_2\text{O}$  (1000 nm (length)

$\times 110$  nm (thickness)), such as those of EP-0, are transformed to pure  $(VO)_2P_2O_7$ , with the apparent shape and size of the crystallites being retained during the transformation at 663 K. However, the resulting  $(VO)_2P_2O_7$  particles were polycrystalline and possessed a double-layered structure consisting of oblong microcrystallites (ca. 50 nm) inside the particle and a distinct shell along the periphery of the particle.

The precursors EP-0, EP-7, EP-15, and EP-36 differed in morphology (size and dimension) but not in bulk crystalline structure. As shown in Figs. 4 and 5, these precursors were transformed into pure  $(VO)_2P_2O_7$ , and the differences in the crystallinity among the resulting  $(VO)_2P_2O_7$  species were negligible. However, the relative intensities and broadness of the diffraction lines in XRD varied for different catalysts (Fig. 4), which suggest a difference in the morphology of the catalyst particles. In fact, SEM images of the catalyst clearly indicated such a difference (Fig. 6).

The apparent shape and size of EC-0 were very similar to those of the corresponding precursor (EP-0, 950 nm (length)  $\times$  200 nm (thickness)), as reported previously [21]. However, the particles of EC-0 are polycrystalline, with a drastic increase in the surface area ( $5 \text{ m}^2 \text{ g}^{-1} \rightarrow 25 \text{ m}^2 \text{ g}^{-1}$ ). In addition, mesopores, attributed to the voids between the crystallites, were present (Fig. 7a). In contrast to this, it should be emphasized that the much smaller precursors EP-7, EP-15, and EP-36, prepared in the mixed alcohol, were transformed into catalysts

consisting of bare, sharply angular, rectangular nano-sized crystallites with sides of about 60 - 170 nm. Their sizes and shapes were quite different from those of the corresponding precursors. In particular, the precursor EP-36 (340 nm (length) × 35 nm (thickness)) formed nano-sized crystallites of  $(VO)_2P_2O_7$  (EC-36, 60 nm (length) × 31 nm (thickness)).

As mentioned above, for moderately sized precursor crystallites, heterogeneous transformation occurred in the crystallite, resulting in the formation of double-layered particles consisting of rectangular microcrystallites (ca. 50 nm) inside the particle and a distinct shell along the periphery of the particle; in contrast, for small-sized precursors, homogeneous transformation, with dehydration, oxidation, and reduction, proceeded in all parts of the crystallite. During such transformations, the crystallites are broken into microcrystallites, due to the difference in the crystal structures of  $VOHPO_4 \cdot 0.5H_2O$  and  $(VO)_2P_2O_7$ , and finally become bare, sharply angular nano-sized  $(VO)_2P_2O_7$  crystallites. As shown in Fig. 3, no large-sized crystallites were present in EP-36, while EP-7 contained crystallites larger than 750 nm. The absence of such large crystallites in EP-36 is the reason for the formation of uniform nano-sized  $(VO)_2P_2O_7$  crystallites in the resulting catalyst (EC-36).

#### *4.3. Influence of catalyst microstructure on selectivity in the selective oxidation of n-butane*

As shown in Fig. 9, EC-7, EC-15, and EC-36 showed higher selectivity to MA for

*n*-butane oxidation compared to EC-0. In particular, EC-36 showed remarkably high selectivity to MA, reaching 78% at low conversion levels, and remaining at 75% even at 80% conversion. In addition, EC-7, EC-15, and EC-36 exhibited high activity (per catalyst weight), about two times higher than that of EC-0. These results demonstrate that the exfoliation-reduction of  $\text{VOPO}_4 \cdot 2\text{H}_2\text{O}$  in a 2-butanol/ethanol mixture produces a highly active and selective catalyst for the oxidation of *n*-butane to MA. The high activity of the catalysts prepared in the mixed alcohol is attributed to their high surface area, since their specific activities per surface area were nearly equal to that of EC-0.

The difference between EC-0 and EC-36 with regard to selectivity toward MA is discussed as a typical example. As shown in Table 2, a comparison of EC-0 and EC-36 shows that both are composed of highly crystalline  $(\text{VO})_2\text{P}_2\text{O}_7$ , and had almost the same bulk oxidation state of V and surface P/V ratio, indicating that the bulk and surface structures of these catalysts were basically the same. However, one striking difference between EC-0 and EC-36 is the state of aggregation of the microcrystallites. The nano-sized crystallites of EC-36 exist separately, and this lack of aggregation results in the absence of mesopores, whereas the crystallites of EC-0 aggregate to form catalyst particles with mesopores. It is speculated that in the gas-phase oxidation of hydrocarbons, further oxidation of the reactants and products to  $\text{CO}_2$  is facilitated in the cavities of micro- and mesopores, in which these components can

remain for long periods. Therefore, the excellent selectivity of EC-36 may be attributed to its lack of such mesopores, which is due to the characteristic state of non-aggregation of the nano-sized  $(VO)_2P_2O_7$  crystallites. Since highly crystalline  $(VO)_2P_2O_7$  shows high selectivity to MA when compared with less crystalline  $(VO)_2P_2O_7$ , it can be assumed that the excellent selectivity observed for EC-36 is due both to its highly crystalline state and to its lack of mesopores.

The selectivities of EC-7 and EC-15 were slightly lower than that of EC-36, but higher than that of EC-0. According to the mesopore size distributions (Fig. 7), neither EC-7 nor EC-15 contain definite mesopores. However, it is possible that a certain number of mesopores exist in EC-7 and EC-15, because the corresponding precursors, EP-7 and EP-15, contained small amounts of largish crystallites, similar to EC-0 (Fig. 3), which are transformed into  $(VO)_2P_2O_7$  particles similar to those of EC-0 and possessing mesopores. For this reason, these catalysts show slightly lower selectivity to MA compared to EC-36.

Hutchings et al. reported that an amorphous VP oxide catalyst ( $VPO_{SCP}$ ) synthesized in supercritical  $CO_2$  was highly active and selective for the selective oxidation of *n*-butane [22,23]. In contrast, EC-50 showed very low activity and selectivity (Table 2), though this was also amorphous. However, it is reasonable that EC-50 was one thing and the material of  $VPO_{SCP}$  is another, because the P/V ratio and oxidation number were quite different; the P/V ratio in the

bulk and oxidation number of V for EC-50 were 1.0 and 4.6, respectively, whereas those for  $VPO_{SCP}$  1.2 ~ 1.5 and 4. The structural difference between two catalysts may be a reason for the difference in the catalytic performances.

## 5. Conclusion

The present study demonstrates that the exfoliation-reduction process of  $VOPO_4 \cdot 2H_2O$  in an alcohol mixture consisting of 2-butanol and ethanol produced small, thin crystallites (340 nm in length and 35 nm in thickness) of  $VOHPO_4 \cdot 0.5H_2O$ , which were transformed into sharply angular nano-sized crystallites (60 nm in length and 31 nm in thickness) of pure  $(VO)_2P_2O_7$ , without mesopores, under the reaction conditions described above. In contrast, the large, thick crystallites (950 nm in length and 200 nm in thickness) of  $VOHPO_4 \cdot 0.5H_2O$  prepared by exfoliation-reduction of  $VOPO_4 \cdot 2H_2O$  in 2-butanol alone were transformed into  $(VO)_2P_2O_7$  particles whose apparent shape and size were very similar to those of the corresponding precursor. The nano-sized crystallites of  $(VO)_2P_2O_7$  formed from the mixed-alcohol precursors exhibited high selectivity toward maleic anhydride in the selective oxidation of *n*-butane, probably due to the absence of mesopores and the highly crystalline state of  $(VO)_2P_2O_7$ .

## **Acknowledgement**

This work was supported by Core Research for Evolution Science and Technology (CREST) of the Japan Science and Technology Corporation (JST).

## References

- [1] G. Centi, F. Trifiró, J. R. Ebner, V. M. Franchetti, *Chem. Rev.* 88 (1988) 55.
- [2] G. Centi, F. Cavani and F. Trifirò, in; *Selective Oxidation by Heterogeneous Catalysis*, (Kluwer Academic, New York, 2001), pp.143.
- [3] G.J. Hutchings, *J. Mater. Chem.* 14 (2004) 3385.
- [4] T. Okuhara, K. Inumaru, M. Misono, *Chem. Lett.* (1992) 1955; T. Okuhara, K. Inumaru, M. Misono, in: S.T. Oyama, J.W. Hightower (Eds.), *Catalytic Selective Oxidation*, in: ACS Symposium Series, Vol. 523, Am. Chem. Society, Washington, DC, 1993, p. 156.
- [5] E. Bordes, *Catal. Today* 16 (1993) 27.
- [6] P.A. Agaskar, L. DeCaul, R.K. Grasselli, *Catal. Lett.* 23 (1994) 339.
- [7] B.K. Hodnett, *Catal. Rev. Eng.* 17 (1985) 373.
- [8] S. Albonetti, F. Cavani, F. Trifiró, *Catal. Rev. Sci. Eng.* 38 (1996) 413.
- [9] T. Shimoda, T. Okuhara, M. Misono, *Bull. Chem. Soc. Jpn.* 58 (1985) 2163.
- [10] G. Busca, F. Cavani, G. Centi, F. Trifiro, *J. Catal.* 99 (1986) 400.
- [11] J.W. Johnson, D.C. Johnson, A.J. Jacobson, J.F. Brody, *J. Am. Chem. Soc.* 106 (1984) 8123.
- [12] L. Benes, K. Melanova, V. Zima, J. Kalousova, J. Votinsky, *Inorg. Chem.* 36 (1997) 2850.
- [13] N. Yamamoto, N. Hiyoshi, T. Okuhara, *Chem. Mater.* 14 (2002) 3882.

- [14] Y. Kamiya, N. Hiyoshi, H. Imai, T. Okuhara, *Catal. Lett.* 111 (2006) 159.
- [15] N. Hiyoshi, N. Yamamoto, N. Ryumon, Y. Kamiya, T. Okuhara, *J. Catal.* 221 (2004) 225.
- [16] T. Nakato, Y. Furumi, N. Terao, T. Okuhara, *J. Mater. Chem.* 10 (2000) 737.
- [17] B.K. Hodnett, P. Permannce, B. Delmon, *Appl. Catal.* 6 (1983) 231.
- [18] M. Abon, K.E. Bere, A. Tuel, P. Delochere, *J. Catal.* 156 (1995) 28.
- [19] Y.E. Gorbunova, S.E. Linde, *Dokl. Akad. Nauk SSSR* 245 (1979) 584.
- [20] C.J. Kiely, A. Burrows, G.J. Hutchings, K.E. Bere, J.C. Volta, A. Tuel, M. Abon, *Faraday Discuss.* 105 (1996) 103.
- [21] Y. Kamiya, N. Hiyoshi, N. Ryumon, T. Okuhara, *J. Mol. Catal. A*, 220 (2004) 103.
- [22] G.J. Hutchings, J.K. Bartley, J.M. Webster, J.A. Lopez-Sanchez, D.J. Gilbert, C.J. Kiely, A.F. Carley, S.M. Howdle, S. Sajip, S. Caldarelli, C. Rhodes, J.C. Volta, M. Poliakoff, *J. Catal.* 197 (2001) 232.
- [23] G.J. Hutchings, J.A. Lopez-Sanchez, J.K. Bartley, J.M. Webster, A. Burrows, C.J. Kiely, A.F. Carley, C. Rhodes, M. Hävecker, A. Knop-Gericke, R.W> Mayer, R. Schlögl, J.C. Volta, M. Poliakoff, *J. Catal.* 208 (2002) 197.

Table 1

Physical and chemical properties of precursors

Precursor	Surface area <sup>a</sup> /m <sup>2</sup> g <sup>-1</sup>	Length <sup>b</sup> /nm	Thickness <sup>c</sup> /nm	Oxidation number of V in bulk <sup>d</sup>	Surface P/V ratio <sup>e</sup>
EP-0	5	950	200	3.97	0.93
EP-7	10	490	100	4.05	1.10
EP-15	15	350	65	3.97	1.09
EP-36	24	340	35	4.07	1.06
EP-50	7	2500	----	3.89	0.87

<sup>a</sup> After pretreatment at 423 K in a vacuum.

<sup>b</sup> Estimated from SEM.

<sup>c</sup> Estimated from the surface area and length [Eq.(1)].

<sup>d</sup> Average oxidation number of vanadium estimated by redox titration.

<sup>e</sup> Estimated from XPS.

Table 2

Physical and chemical properties of catalysts, and catalytic activity and selectivity for *n*-butane oxidation

Catalyst	Surface area <sup>a</sup> /m <sup>2</sup> g <sup>-1</sup>	Length <sup>b</sup> /nm	Thickness <sup>c</sup> /nm	Oxidation number of V in bulk <sup>d</sup>	Surface P/V ratio <sup>e</sup>	Activity <sup>f</sup> /10 <sup>-4</sup> mol g <sup>-1</sup> h <sup>-1</sup>	Selectivity <sup>g</sup> /%
EC-0	25	620	26	4.04	1.26	18 (0.72)	71.6 (40.6)
EC-7	35	170	21	4.02	1.20	32 (0.92)	75.3 (42.7)
EC-15	37	120	22	4.04	1.32	32 (0.86)	76.2 (39.6)
EC-36	40	60	31	3.99	1.20	31 (0.79)	78.4 (42.4)
EC-50	6	1300	----	4.57	1.08	3 (0.41)	21.3 (21.7)

<sup>a</sup> After pretreatment at 423 K in a vacuum.<sup>b</sup> Estimated from SEM.<sup>c</sup> Estimated from the surface area and length [Eq.(1)].<sup>d</sup> Average oxidation number of vanadium estimated by redox titration.<sup>e</sup> Estimated from XPS.<sup>f</sup> Values in parentheses represent the specific activity per surface area (10<sup>-4</sup> mol m<sup>-2</sup> h<sup>-1</sup>).<sup>g</sup> Values in parentheses are the conversion at which selectivity was measured.

## Figure captions

**Fig. 1** XRD patterns of the precursors. (a) EP-0, (b) EP-7, (c) EP-15, (d) EP-36, and (e) EP-50. ●,  $\text{VOHPO}_4 \cdot 0.5\text{H}_2\text{O}$ .

**Fig. 2** IR spectra of the precursors. (a) EP-0, (b) EP-7, (c) EP-15, (d) EP-36, and (e) EP-50.

**Fig. 3** SEM images of the precursors and starting material ( $\text{VOPO}_4 \cdot 2\text{H}_2\text{O}$ ), and size distributions of the precursor crystallites. (a) EP-0, (b) EP-7, (c) EP-15, (d) EP-36, (e) EP-50, and (f)  $\text{VOPO}_4 \cdot 2\text{H}_2\text{O}$ .

**Fig. 4** XRD patterns of the catalysts. (a) EC-0, (b) EC-7, (c) EC-15, (d) EC-36, and (e) EC-50. □,  $(\text{VO})_2\text{P}_2\text{O}_7$ .

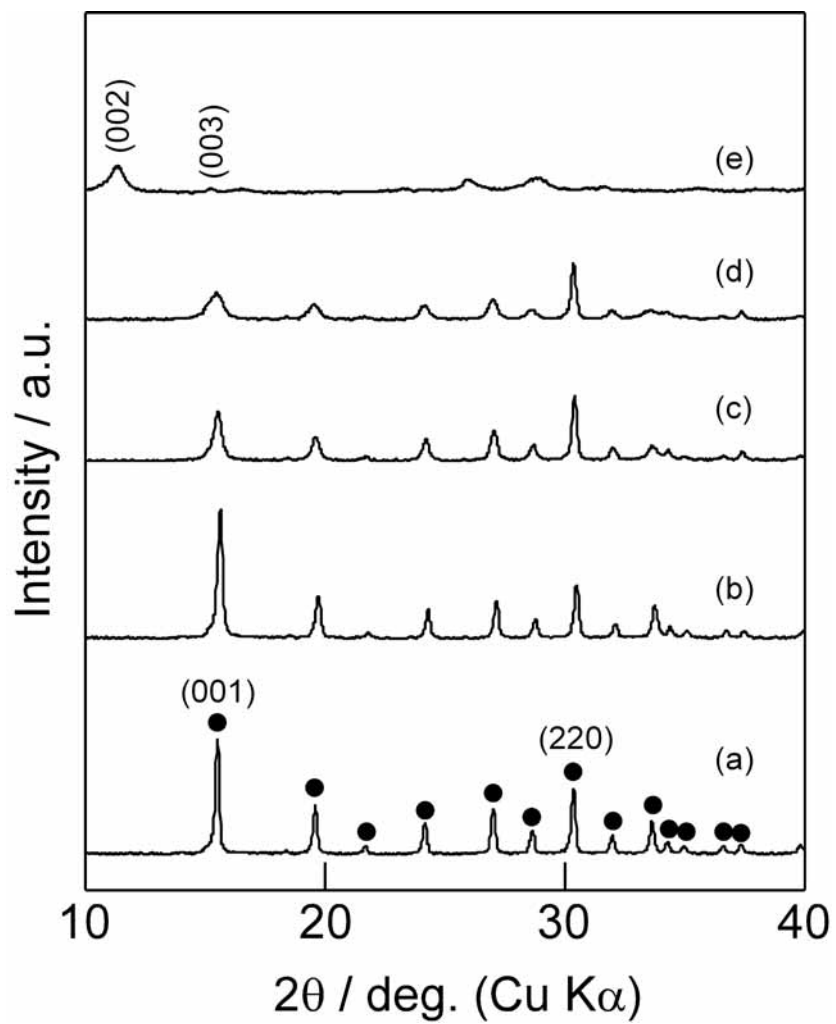
**Fig. 5** IR spectra of the catalysts. (a) EC-0, (b) EC-7, (c) EC-15, (d) EC-36, and (e) EC-50.

**Fig. 6** SEM images and particle size distributions of the catalysts. (a) EC-0, (b) EC-7, (c) EC-15, (d) EC-36, and (e) EC-50.

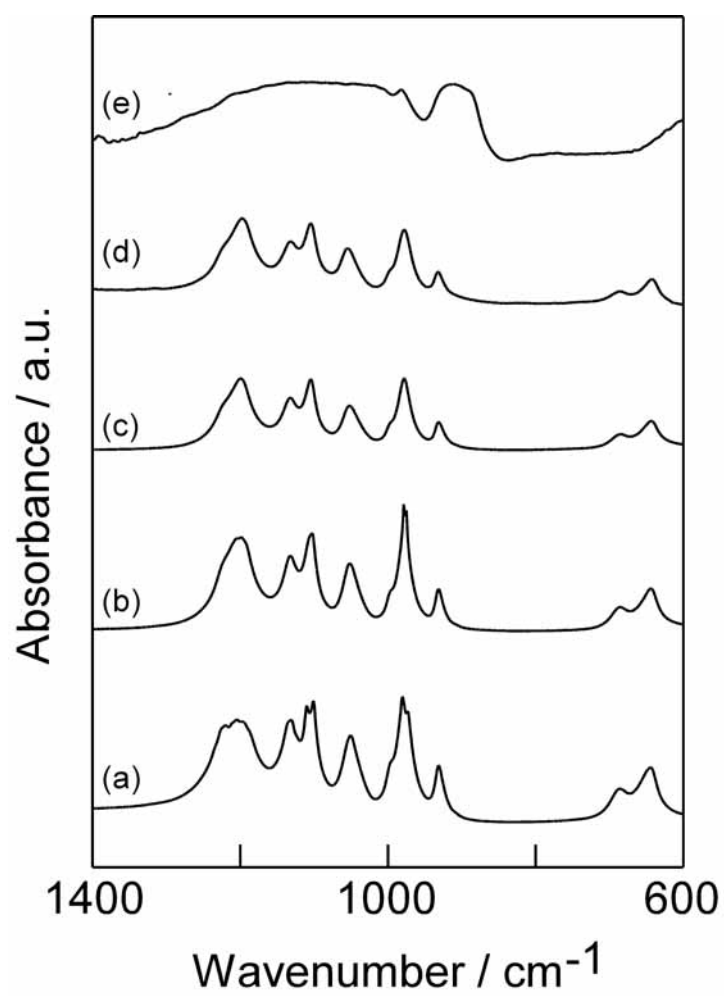
**Fig. 7** Mesopore size distributions of the catalysts. (a) EC-0, (b) EC-7, (c) EC-15, (d) EC-36, and (e) EC-50.

**Fig. 8** *W/F* dependence for conversion of *n*-butane: (○) EC-0, (□) EC-7, (■) EC-15, and (●) EC-36. The reaction was performed at 703 K with a mixture of *n*-butane (1.5%),  $\text{O}_2$  (17%), and He (balance). The data were collected after 150 h of reaction.

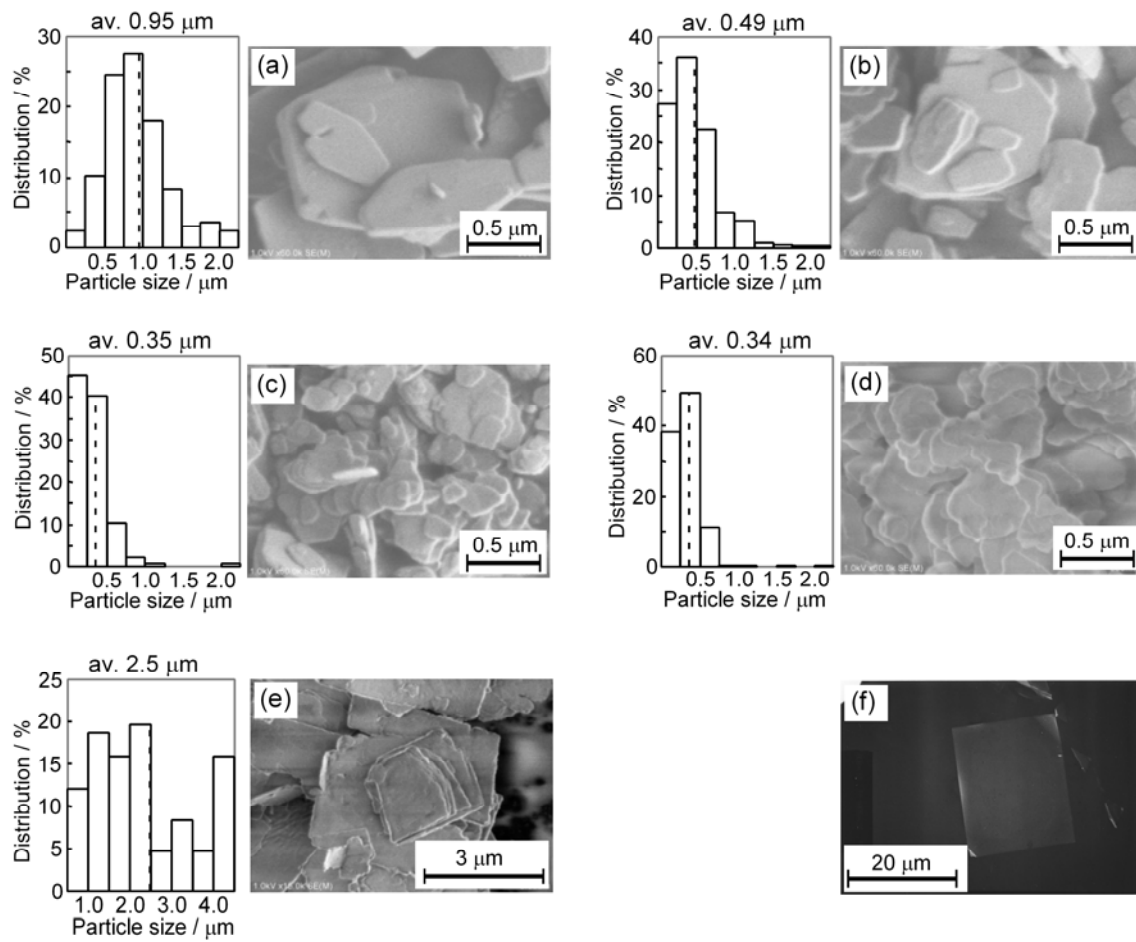
**Fig. 9** Selectivity toward maleic anhydride (MA) as a function of conversion of *n*-butane: (○) EC-0, (□) EC-7, (■) EC-15, and (●) EC-36. The reaction was performed at 703 K with a mixture of *n*-butane (1.5%),  $\text{O}_2$  (17%), and He (balance). The data were collected after 150 h of reaction.



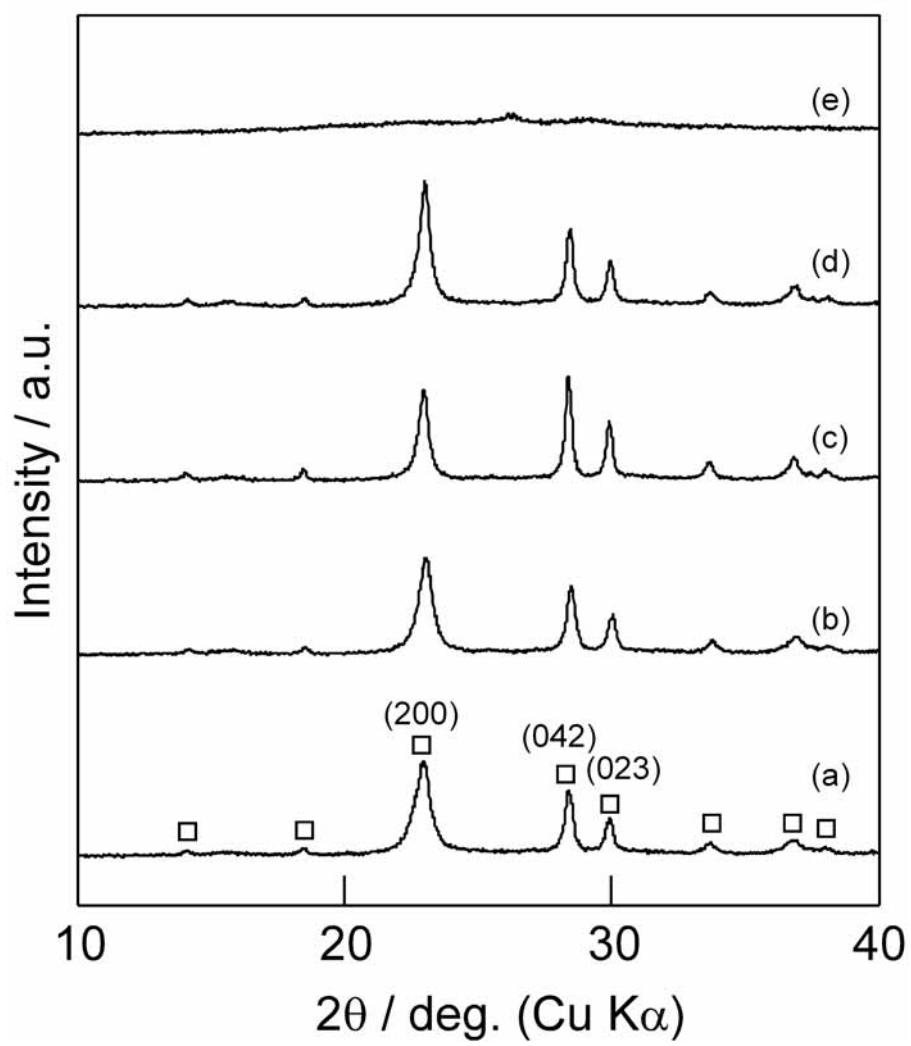
Imai et al.  
Fig. 1



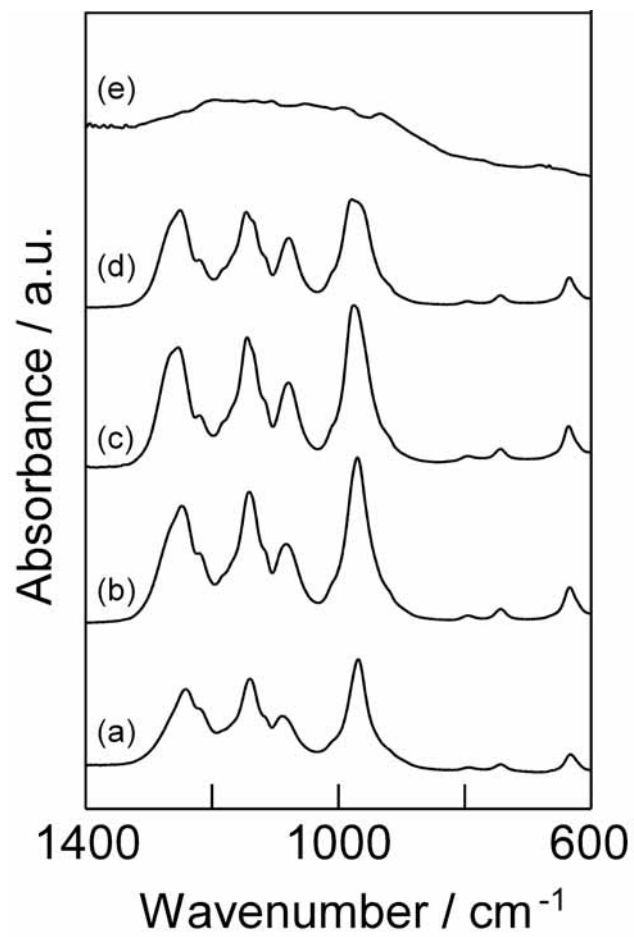
Imai et al.  
Fig. 2



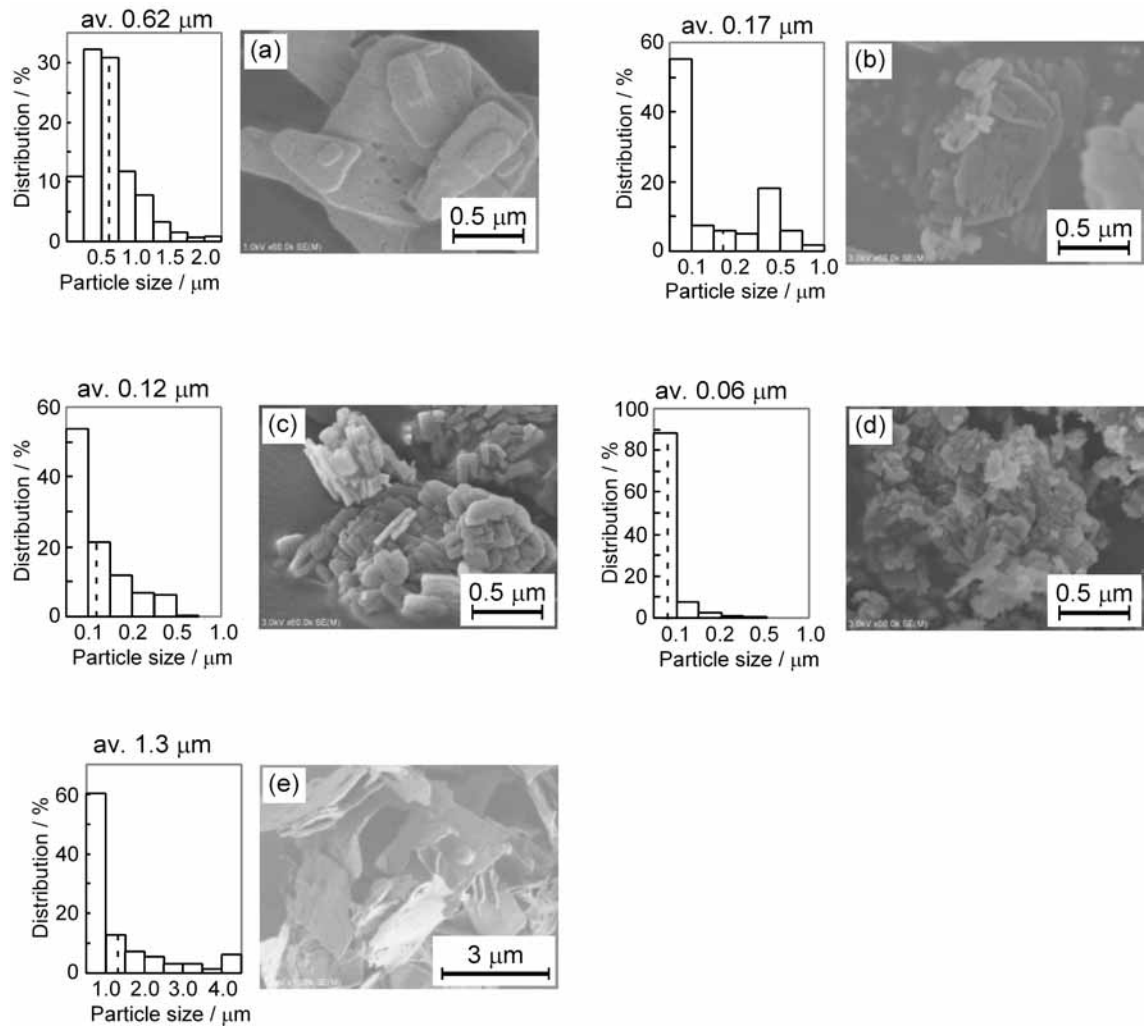
Imai et al.  
 Fig. 3



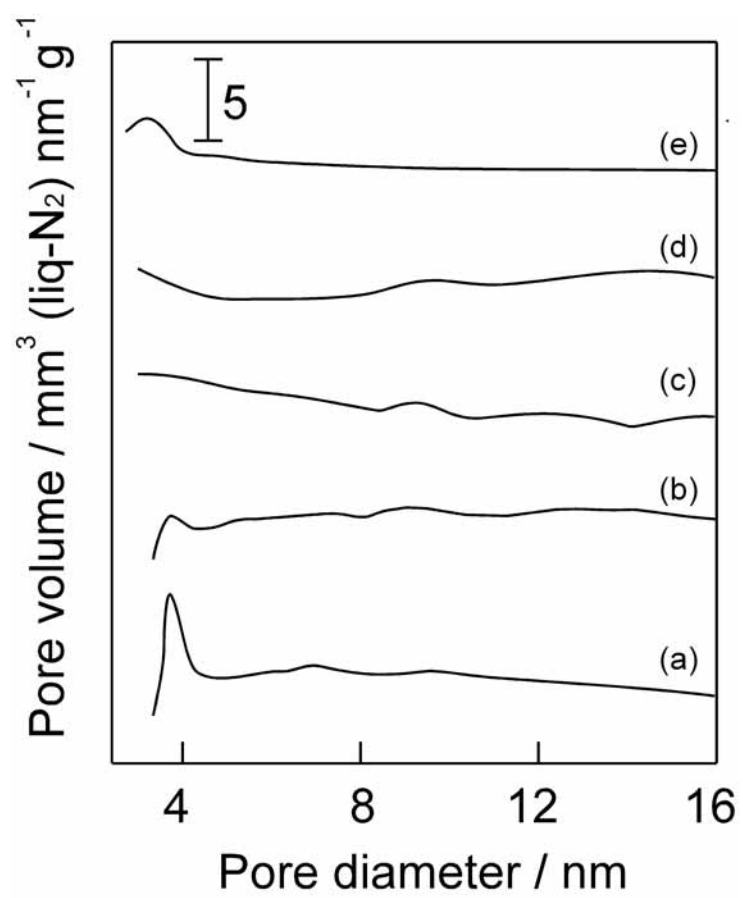
Imai et al.  
Fig. 4



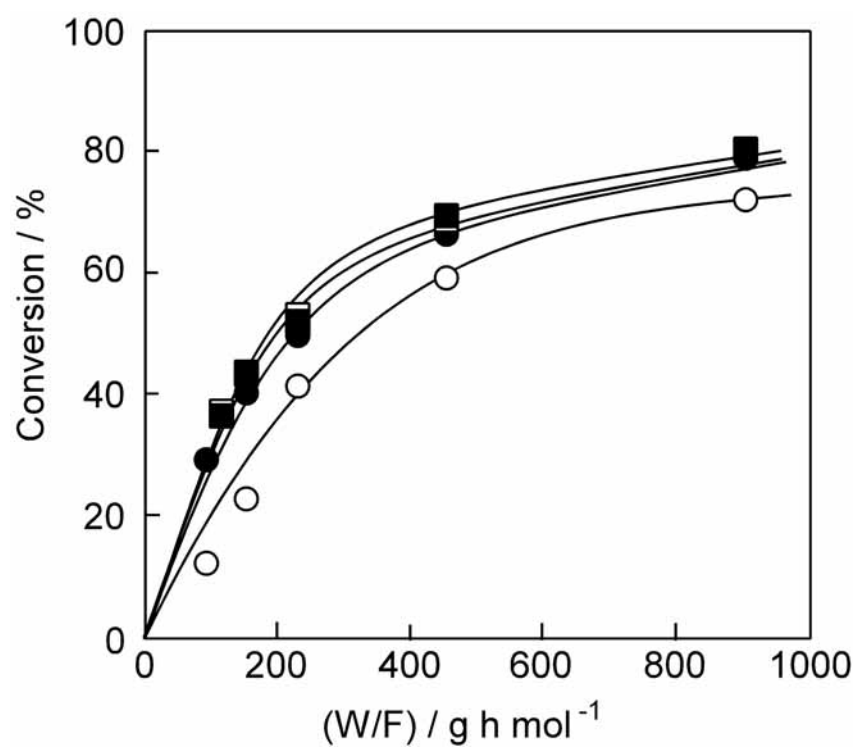
Imai et al.  
Fig. 5



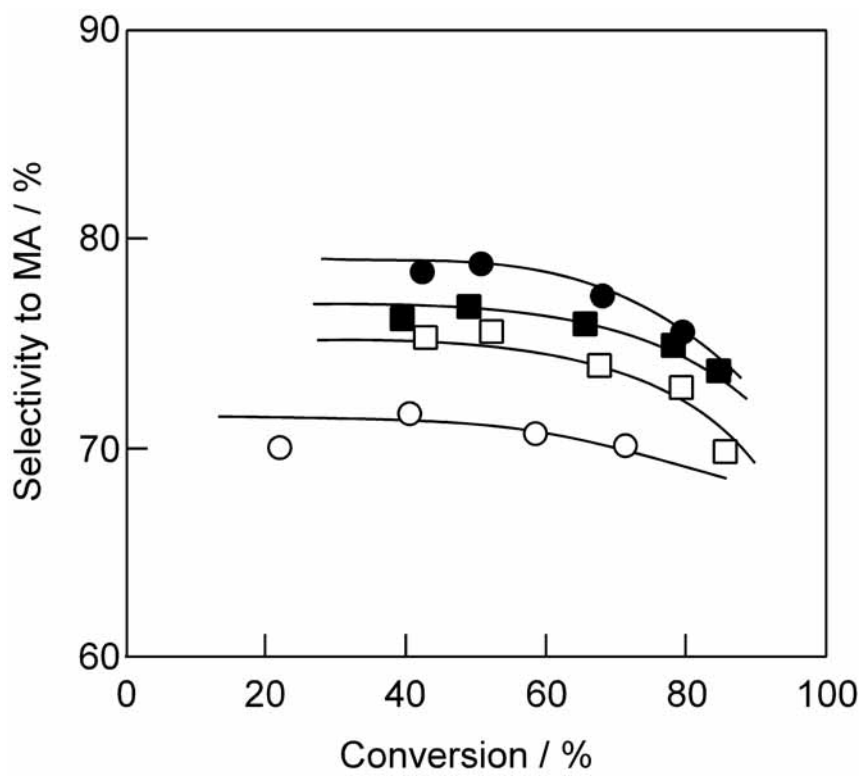
Imai et al.  
Fig. 6



Imai et al.  
Fig. 7



Imai et al.  
Fig. 8



Imai et al.  
Fig. 9